

Nitrogen-doped hollow carbon spheres as chemical vapour sensors

Bridget K. Mutuma^{a,c*}, Clara I. Garcia-Martinez^b, Rodrigo C. Dias^b, Boitumelo J. Matsoso^{ad}, Neil J. Coville^a,
and Ivo A. Hümmelgen^{b*}

This study reports on low nitrogen content-doped hollow carbon spheres (N-HCSs) for use as chemical vapour sensors. The N-HCSs were prepared by a template-assisted chemical vapour deposition method followed by nitrogen doping in an ammonia atmosphere. Raman spectroscopy displayed an increase in the I_D/I_G ratio of the carbons upon N-doping indicating the creation of structural defects in the hollow carbon spheres (HCSs). The XPS results showed the N-HCSs had a very low N content (0.6 at. %) comprising predominantly pyridinic-N (35%) and pyrrolic-N (48%) configurations. The XPS results showed the N-HCSs had a very low N content (0.6 at. %) comprising predominantly pyridinic-N (35%) and pyrrolic-N (48%) configurations. Annealed HCSs obtained by thermal annealing in Ar exhibited a lower I_D/I_G ratio and higher thermal stability than the N-HCSs. The HCSs-based sensors were exposed to varying concentration of acetone, water, lactic acid, ammonia, toluene, chloroform and methanol vapours at room temperature. Low detection limits for toluene (15 ppm), lactic acid (12 ppm) and ammonia (6 ppm) were established for the N-HCSs-based sensors. The methanol sensitivity for the N-HCSs was recorded to be 150 times higher than that of related rGO based sensors. This was ascribed to the moderate degree of graphitization, hollow carbon morphology and the electron-rich N-HCSs surface. Most importantly, the water dependency for the N-HCSs was lower than that of the un-doped HCSs. This indicated the effect of heat treatment and post-nitrogen doping of the HCSs in significantly lowering the humidity dependency of the carbons. Thus, the results suggested that the N-HCSs nanostructures are potential candidates for humidity-insensitive environmental sensing devices for the detection of various chemical vapours.

1. Introduction

Hollow carbon spheres are interesting nanomaterials that possess unique textural, morphological and structural properties^{1,2,3}. The hollow carbon spheres (HCSs) have been synthesized by various procedures such as the hydrothermal method⁴, pyrolysis⁵ and templating methods^{6,7}, among others. The templating process has gained much attention due to the ease of synthesis and the cost-effectiveness of the method. A typical template is made of SiO_2 . This is a hard template, that allows for the tunability of the sphere size and surface area and yields a controlled carbon morphology after template removal^{8,9}. Recent reports have indicated that the ability to control the carbon nanosphere morphology can also be readily achieved by pyrolysis and carbonization of polymer templates^{10,11,12}. For instance, the carbon shell thickness that is

formed on a template can be controlled by varying the surfactant to precursor ratio^{13,14}, the amount of the carbon source¹⁵ and the carbonization time¹⁶. A longer carbonization time and a larger amount of a carbon source result in the formation of a thicker carbon shell whereas a shorter carbonization time will yield a thinner carbon shell¹⁷. The change in the HCSs shell thickness can influence their degree of graphitization and the conductivity of the carbon layer¹⁸. Owing to their interesting structural, electrical, surface and catalytic properties, HCSs have been applied in supercapacitors¹⁹, as sensors^{20,21}, in catalysts³ and in fuel cells². Most importantly, the surface groups, the surface porosity and the conductivity have been found to influence the sensing properties of porous carbons and HCSs^{20,21}.

Typically, the conductivity and reactivity of carbon materials can be enhanced by doping them with heteroatoms such as nitrogen and boron^{22,23}. For example, the introduction of nitrogen atoms into the lattice of the carbon materials can be achieved by the use of nitrogen-containing precursors^{24,25,26}. This can occur via an in-situ N-doping process whereby pyrolysis of both the carbon and the nitrogen-containing precursors occurs simultaneously resulting in the growth of N-doped carbon materials²⁷. In contrast, a post-synthesis N-doping process can also be used, whereby the carbon

^a DST-NRF Centre of Excellence in Strong Materials and the Molecular Sciences Institute, School of Chemistry, University of the Witwatersrand, WITS 2050, Johannesburg, South Africa.

^b Departamento de Física, Universidade Federal do Paraná, Caixa Postal 19044, 8153-980 Curitiba, PR, Brazil.

^c Department of Physics, Institute of Applied Materials, University of Pretoria, 0028, Pretoria, South Africa. E-mail: bridgetmutuma@gmail.com; Tel: +2712-420-6780

^d Laboratoire des Multimatériaux et Interfaces, UMR-5615 CNRS, Université Claude Bernard Lyon 1, Villeurbanne-Cedex 69622, France

materials are annealed at high temperatures in the presence of nitrogen-containing compounds such as ammonia, urea, melamine, polypyrrole or acetonitrile, among others^{28,29,30,31}. In both cases, the electronic and catalytic properties of N-doped carbons are influenced by the amount of N-doping and the type of N-configuration found on the carbon surface^{32,33,34,35}.

Recently, nitrogen doping of porous carbons has been reported to lead to enhanced gas sensing properties due to improved electrical/charge conductivity³⁶. As the sensing of gases involves a change in the electron donating or electron accepting properties of the sensing element, an addition of electrons from nitrogen or other heteroatoms in the carbon matrix could thus result in a change in conductivity. In addition, the type of nitrogen configuration found on the carbon surface can significantly influence the charge transfer, gas molecule-carbon surface interaction, surface wettability and the selectivity of gas molecules^{37,38,39}. For instance, Adjizian *et al.*³⁸ reported on the enhanced NO₂ and CO sensing properties of N-doped carbon nanotubes (N-CNTs) compared to related pristine CNTs. They attributed this to the presence of a 2.2 at.% of nitrogen content that created more defects on the CNT-matrix and a better gas molecule-CNT surface interaction. The NO₂ and CO gas molecules were found to bind more strongly to the nitrogen-vacancy defects (pyridinic-N and pyrrolic-N) than to the substitutional-N (graphitic-N) sites. Similarly, Battie *et al.*⁴⁰ reported an improved charge transfer and enhanced ammonia sensitivity after using N-doped single-walled carbon nanotubes (1.2 at. % N). The presence of a strong interaction between the pyridinic-N and the ammonia molecules enhanced the charge transfer properties and the overall sensor response. In addition, the N-doped hollow carbon spheres have been explored as electrochemical sensors due to their tunable porosity, surface reactivity caused by the nitrogen defects and the ease of modification of the carbon matrix polarity^{41,42,43,44}.

The sensing of volatile organic compounds by nanomaterials is greatly hindered by the cross-sensitivity to other volatile molecules and particularly water vapour. Indeed, the chemical vapour sensing properties of metal oxides and carbon-based materials are highly influenced by relative humidity^{45,46,47}. For carbon-based sensors, the presence of amorphous carbon domains and sp²/sp³ carbon “dangling bonds” can affect the wettability of the carbon. The carbon domains tend to possess a high affinity for water molecules leading to cross-sensitivity and compromised performance^{48,49,50}. Previous reports have shown that heat treatment of carbons can reduce the cross-sensitivity and result in a humidity-independent chemical vapour sensor⁵¹. However, heat treatment also has the potential of removing nitrogen atoms from N-doped carbons as well as surface oxygen groups which ultimately leads to a lower N/C ratio and consequently, compromised sensitivity.

To address this issue, post-synthesis nitrogen doping has been adopted as a promising route to facilitate both heat treatment as well as the introduction of dopants into the carbon lattice. The use of nitrogen-containing precursors such as acetonitrile or urea results in the creation of a new carbon doped layer on the pristine carbon surface giving a carbon core@carbon/nitrogen shell nanostructure³⁰. The additional carbon/nitrogen layer can introduce amorphous carbon domains which have a high affinity for water molecules (humidity), thus limiting the overall performance of these carbon-based sensors. Therefore, the use of a nitrogen-rich source, devoid of carbon atoms, as well as heat treatment could aid in reducing the humidity-dependent sensing properties of carbon nanomaterials.

In this study, we report on the use of ammonia gas as the high purity nitrogen source for the post-synthesis nitrogen doping of hollow carbon spheres (N-HCSs). While the use of N-doped porous carbons and N-CNTs in gas/vapour sensing^{51,52,38} have been widely explored, the application of N-doped HCSs in such technological devices, to our knowledge, is as yet to be reported. Therefore, as a proof of concept, the sensing properties of the N-HCSs towards a diverse range of analytes (water, lactic acid, ammonia, methanol, acetone, toluene and chloroform) with varying analyte concentration was investigated. The doping of the HCS was found to influence the humidity sensing ability of the carbons.

2. Experimental

2.1 Starting materials

Silica spheres were synthesized using tetraethyl-orthosilicate, TEOS (98%, Aldrich), ammonium hydroxide, NH₄OH (25%), ethanol (96%, Aldrich) and deionized H₂O (resistivity > 18.2 MΩ cm⁻¹). Hydrofluoric acid (HF; 40%, Associated Chemical) and toluene (99.8%, Aldrich) were used for the preparation of hollow carbon spheres. The argon (Ar, 99.9%) and ammonia (NH₃, 10% in Ar) gases were supplied by Afrox, South Africa.

2.2 Synthesis of SiO₂ spheres and N-HCSs

The SiO₂ spheres were synthesized following a modified procedure reported elsewhere¹⁷. Briefly, 180 mL of ethanol, 60 mL of distilled water and 10 mL of NH₄OH were mixed in a volumetric flask and stirred for 30 min. Then 32 mL of TEOS was added rapidly and the mixture was stirred for another 2 h. The resulting solution was centrifuged at 7000 rpm for 10 min and the precipitate washed three times with a distilled water and ethanol mixture to remove unused reactants. The collected product was dried in an oven overnight at 80 °C. Carbonization of the SiO₂ spheres was carried out in a horizontal CVD reactor at 900 °C for 2 h by a bubbling method using toluene as the carbon source and argon as the carrier gas. The carbonized silica spheres were then etched with 10% HF for 24 h at room temperature, washed several times and dried to give the pristine HCSs. Further heat treatment of the

pristine HCSs was performed at 600 °C for 1 h under Ar gas to give the annealed HCSs. The post-synthesis N-doping of the pristine HCSs was carried out in a CVD reactor at 600 °C for 1 h using 10 sccm or 50 sccm ammonia gas to give N-HCSs-10 or N-HCSs-50, respectively.

2.3 Characterization of the HCSs

The morphology of the annealed HCSs and N-HCSs was evaluated using a FEI TEM Technai G2 spirit electron microscope operating at 120 keV. The Raman spectra of the HCSs were measured at ambient conditions using a Jobin-Yvon T6400 micro-Raman spectrometer equipped with a laser excitation wavelength of 532 nm and a liquid N₂ cooled charge-coupled device detector. The thermal stability of the HCSs was investigated by a thermogravimetric analysis (TGA) instrument conjugated with a weight loss derivative curve (DTG) using a Perkin Elmer Pyris 1 TGA. A 10 mg sample was placed in a ceramic pan and heated from 35 °C to 900 °C at a rate of 10 °C/min under air (10 mL/min) in the instrument furnace. The N₂ adsorption and desorption isotherms of the HCSs were taken at 77 K using a Micrometrics Tristar 3000 instrument. The samples were degassed at 150 °C in a N₂ atmosphere for 4 h. The specific surface area was calculated by the BET method from N₂ adsorption data. The chemical composition of the HCSs was determined by X-ray photoelectron spectroscopy (XPS, Thermo ESCALab 250) using a monochromatic Al K α X-ray source with an X-ray power of 300 W and a spot size of 900 μ m.

2.4 Preparation of the sensing devices

Devices fabricated with the annealed HCSs, N-HCSs-10 and N-HCSs-50 were screened with different apolar and polar (protic and aprotic) analytes (water, lactic acid, ammonia, methanol, acetone, toluene and chloroform) to evaluate their chemical vapour sensing properties (Table 1).

Table 1: Properties of the various analytes⁵³

Analyte	Nature of Solvent	Dielectric constants (ϵ)	Dipole moment (D)	Vapour pressure (kPa)
Water	Polar protic	78.5	1.85	3.16
Lactic acid	Polar protic	22.0	-	0.007
Ammonia	Polar protic	25.0	1.46	49.6
Methanol	Polar protic	32.6	1.70	16.9
Acetone	Polar aprotic	17.7	2.88	30.6
Toluene	Apolar	2.4	0.36	3.79
Chloroform	Apolar	4.8	1.12	22.62

The three types of HCSs were separately dispersed in water using hexadecyltrimethylammoniumbromide (CTAB) as a surfactant at a N-HCSs:CTAB ratio of 1:2 w/w, as reported elsewhere²¹. The N-HCSs dispersion was then deposited on an FR4 substrate containing the interdigitated electrodes (ENIG-Electroless Nickel Immersion Gold, supplied by Micropress S.A.) with an active area of 7.9 mm \times 8 mm and a separation of 0.1 mm between the electrodes strips⁵⁴. The dispersion (100

μ L) was drop casted on the interdigitated electrode followed by drying in an oven for 30 min at 100°C. An LCR meter (Agilent 4284A) was used for the resistance measurements, which were carried out under steady-state condition using a 2 L glass flask containing the analyte vapour. The analyte solutions of varying volumes (corresponding to the vapour concentrations) were dropped using a micropipette into the sealed glass flask. The vapour concentration of the various analytes ($C(ppm)$) was determined from the volume of each analyte added using the equation 1 below⁵⁵;

$$C(ppm) = \frac{2.46Vd}{VsMw} \times 10^7 \quad (1)$$

Where V represents the volume added in μ L, d is the density of analyte in gM^{-1} , V_s is the volume of the chamber in mL (in this case 2000 mL) and M_w is the molecular weight of analyte solution in gM^{-1} . The concentration of the analyte was varied but no further sensor optimization studies were performed regarding sensor geometry, dispersion conditions or amount of material used. The sensing performance was determined based on the limit of detection (LoD) and the sensitivity (S), where $LoD = R_b + 3d_b$ ⁵⁶ and $S = dResp/dC$ (R_b is the average and d_b the standard deviation of the device resistance without analyte, respectively). For the response, $Resp$, the relative variation of the resistance was used, i. e., $Resp = \Delta R/R_0 = (R_f - R_0)/R_0$ (R_f is the resistance of the sensor when exposed to analyte and R_0 the resistance of the sensor under a dry N₂ atmosphere).

3. Results and discussion

3.1 Morphological and structural properties of the HCSs and N-HCSs

Figure 1 shows the TEM images for the annealed HCSs and N-HCSs. The annealed HCSs have an inner diameter of 435 ± 12 nm and a shell thickness of ~ 25 nm (Figure 1a). The HCSs inner diameter was similar to that of the silica sphere template used (438 ± 16 nm; Figure S1a-b). After N-doping the N-HCSs had thin shells (~ 24 nm for N-HCSs-10; ~ 22 nm for N-HCSs-50) (Figure 1b and 1c) and a few broken HCSs were observed in the N-HCSs-50 sample (Figure S1c). This suggests that a high ammonia concentration can result in etching of the carbon atoms in the N-HCSs. Indeed, a similar etching effect by the ammonia gas has been observed in nitrogen-doped graphene oxide⁵⁷ as well as in cellulose-derived carbon aerogels⁵⁸. This can be explained by the ammonia gas reacting with the oxygen functional groups on the carbon surface, replacing them with nitrogen-containing groups^{57,58}. The decomposition of ammonia could also result in the generation of active radicals that etch the carbon atoms^{59,60}.

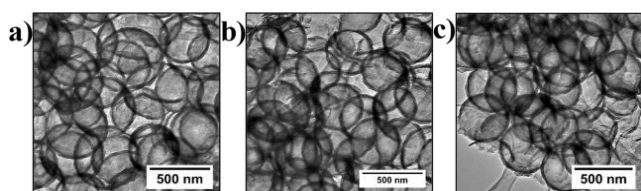


Figure 1: TEM images of, (a) annealed HCSs, (b) N-HCSs-10 and (c) N-HCSs-50.

Figure S2a shows the thermal gravimetric curves of the annealed HCSs and N-HCSs. The onset decomposition peaks were at 515 °C, 508 °C and 492 °C for the annealed HCSs, N-HCSs-10 and N-HCSs-50, respectively. The decrease in decomposition temperatures of the HCSs further suggested the reduction of thermal stability after ammonia treatment. The absence of decomposition peaks at lower temperatures (< 400 °C) in both the HCSs and N-HCSs indicated the lack of amorphous carbon domains that could emanate from mainly sp^3 hybridized carbons and nitrogen bonded to sp^3 hybridized carbon^{30,61}. This is expected as the heat treatment and doping was carried out in argon or ammonia atmospheres at 600 °C. Interestingly, the derivative profiles of the N-HCSs were broader (FWHM; N-HCSs-10: $80.0 \pm 0.2 \text{ cm}^{-1}$ and N-HCSs-50: $116.5 \pm 0.3 \text{ cm}^{-1}$) than those of the annealed HCSs (Figure 2a). The narrow derivative peak (FWHM: $61.6 \pm 0.2 \text{ cm}^{-1}$) of the annealed HCSs can be attributed to the presence of a higher degree of graphitic carbon^{21,62}. In contrast, the broadness of the derivative peaks in the N-HCSs can be attributed to the presence of defects induced by nitrogen incorporated into the carbon matrix. Moreover, the presence of nitrogen-containing active radicals due to ammonia decomposition, can result in different decomposition rates yielding broader derivative peaks in the N-HCSs.

Table 2: Raman band positions, I_D/I_G ratio and BET surface areas of the HCSs

Material	D band position (cm^{-1})	G band position (cm^{-1})	I_D/I_G ratio	BET Surface areas (m^2g^{-1})
Annealed HCSs	1344	1586	0.51	55.8 ± 0.7
N-HCSs-10	1338	1588	0.53	81.7 ± 0.5
N-HCSs-50	1346	1594	0.72	87.6 ± 1.0

Raman spectroscopy was used to study the graphitic nature of the annealed HCSs and N-HCSs. Figure 2b shows the Raman spectra of the HCSs and N-HCSs with D peaks observed between 1338 cm^{-1} and 1346 cm^{-1} , respectively. The D peak is associated with the breathing mode of sp^2 carbon atoms and the presence of defects in the carbon structure⁶³. The G peak observed between 1586 cm^{-1} and 1594 cm^{-1} is due to the E_{2g} mode of vibration of sp^2 bonded carbon and bond stretching of sp^2 atoms^{30,64}. A slight upshift of the G peak was observed (Table 2) in the N-HCSs and can be ascribed to the nitrogen-induced defects incorporated within the carbon lattice^{30,65}. The annealed HCSs gave a low I_D/I_G ratio (0.51) indicating that the HCSs had a moderate degree of graphitization. The I_D/I_G ratio increased with increasing doping concentration ($0.53_{\text{N-HCSs-10}}$

versus $0.72_{\text{N-HCSs-50}}$). This indicates that more structural defects were introduced at the higher ammonia concentration (50 sccm) compared to when a lower ammonia concentration (10 sccm) was used.

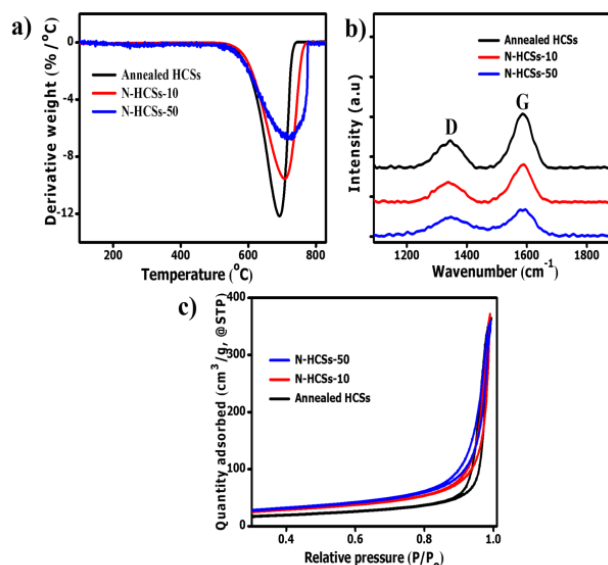


Figure 2: (a) Thermal gravimetric derivative profiles, (b) Raman spectra and (c) N_2 - adsorption and desorption isotherms of the annealed HCSs and N-HCSs.

The N_2 adsorption and desorption isotherms show a type (III) isotherm with a H3 hysteresis loop at a relative pressure of $P/P_0 = 0.85 - 1.0$ for all three samples (Figure 2c). This indicated an assemblage of slit-shaped pores or plate-like particles for both samples⁶⁶. The BET surface area was calculated to be $55.8 \pm 0.7 \text{ m}^2\text{g}^{-1}$, $81.7 \pm 0.5 \text{ m}^2\text{g}^{-1}$ and $87.6 \pm 1.0 \text{ m}^2\text{g}^{-1}$ for the annealed HCSs, N-HCSs-10 and N-HCSs-50, respectively. The low surface areas of the HCSs can be ascribed to the non-porous silica spheres used as templates. However, the BET surface area of N-HCSs was larger than that of the annealed HCSs. The small increase could be linked to the incorporation of nitrogen atoms within the carbon matrix⁶⁷ as well as the formation of pores on the carbon surface upon the reaction of active radical species with carbon. Moreover, the decomposition of ammonia generates radicals that react with and erode some of the carbon fragments and so create more pores within the N-doped carbon structure, thus increasing the specific surface area^{59,60}. The pore size distribution plots for the annealed HCSs and N-HCSs are shown and discussed in the supplementary section (Figure S2b).

3.2 XPS analysis of the N-HCSs

The integral peak areas of the XPS survey spectra were used to determine the elemental composition (at.%) of the annealed HCSs and the N-HCSs (Table 3). As expected no nitrogen was present in the annealed HCSs and the carbon content was higher than that in the N-HCSs. After N-doping the carbon contents decreased with increasing dopant concentration (ammonia), indicating successful incorporation of nitrogen

atoms, either via the substitution of carbon with nitrogen or through the formation of nitrogen-induced defects within the carbon matrix. Furthermore, XPS data revealed that on increasing the amount of dopant (N-HCSs-50), the nitrogen content was increased to ≈ 0.6 at %, in comparison to the nitrogen content of 0.2 at % for the N-HCSs-10 (Table 3). Thus, the use of the higher ammonia dopant concentration (50 sccm) gave a satisfactory amount of nitrogen on the carbon surface, leading to an increase in surface area and defective N-doped carbon structures; a sought-after property desirable for sensing applications. The lower nitrogen content resulted from a low reaction efficiency between the carbon matrix and ammonia. The annealed HCSs had the lowest oxygen content ≈ 2 at. % owing to the removal of oxygenated functional groups at high temperature treatment in Ar gas. As for the N-HCSs, the N-HCSs-10 had a slightly higher oxygen content than the N-HCSs-50 due to the incorporation of fewer nitrogen-containing groups at lower ammonia concentration. Thus, an oxygen content of ≈ 3 at.% was recorded for the N-HCSs. This can be attributed to the removal of oxygen-containing groups during the annealing process in NH_3 gas that simultaneously resulted in the N-doping of the carbon matrix. Typically, the presence of few oxygen-containing groups on a carbon surface is expected to limit the amount of nitrogen incorporated into the carbon matrix⁶⁸. Oxidized carbon on the surface has a high affinity for water and thus, could hinder the chemical sensing efficiency of non-water analytes.

Table 3: Atomic compositions of the annealed HCSs and N-HCSs

Samples	C (at. %)	N (at. %)	O (at. %)
Annealed HCSs	98.3	-	1.7
N-HCSs-10	97.0	0.2	2.8
N-HCSs-50	96.7	0.6	2.5

High resolution C1s XPS spectra of annealed HCSs (Figure S2c) and N-HCSs (Figures 3a and c) exhibited an asymmetrical and tailing peak, which is indicative of different bonding states for the C atoms, comprising of sp^3 and sp^2 hybridized carbons. The binding energy region at ≈ 285.0 eV corresponding to the sp^3 C-C bonds and the lower binding energy region located at ≈ 284.0 eV is ascribed to the sp^2 C=C bonds of graphite⁶⁹. In both N-HCSs-10 and N-HCSs-50, two additional peaks were observed at 284.8 - 284.9 eV and 285.8 - 285.9 eV. These binding energies can be attributed to the bonding of the carbon atoms (*c.a.* 2.55) to more electronegative nitrogen atoms (*c.a.* 3.04), thus forming sp^2 C=N and sp^3 C-N bonding configurations, respectively⁷⁰. Finally, component peaks located at a higher binding energy of 286.0 eV and 289.0 eV correspond to the presence of C-O and O-C=O bonds in HCSs, whereas for the case of N-HCSs, these signified the presence of C-O and N-C=O bond⁶⁵.

The N1s spectrum of the N-HCSs was deconvoluted into four component peaks. The peak centered at 398.1 eV and 397.9 eV in the N-HCSs-10 and N-HCSs-50, respectively, was assigned to pyridinic-N (with the N atom contributing one electron to

the π -system). The pyrrolic-N, graphitic-N and NO_x peaks were centered at 399.4 eV, 400.8 eV and 402.2eV in the N-HCSs-10 (Figure 3b). In the N-HCSs-50, these three component peaks were centered at 399.3 eV, 400.4 eV and 402.0 eV, respectively (Figure 3d). The pyrrolic-N contributes two electrons to the π -system while in the graphitic-N, the N atom substitutes the C atom in the graphitic structure⁷¹.

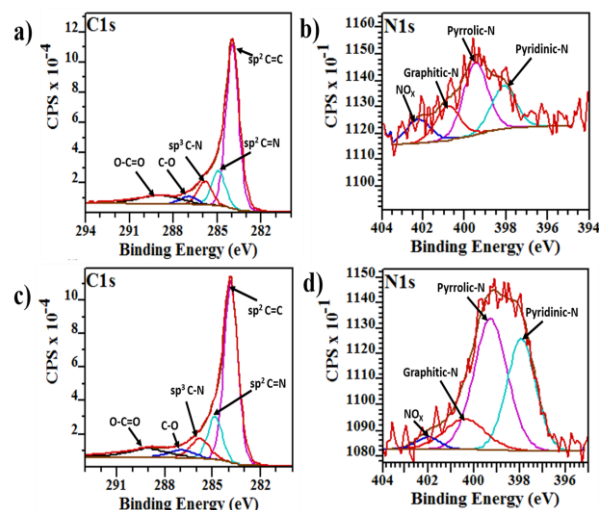
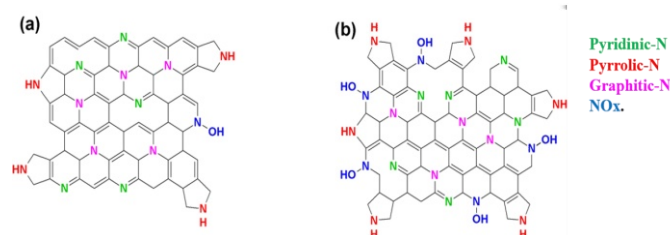


Figure 3: The XPS spectra of deconvoluted C1s and N1s peaks; (a-b) N-HCSs-10 and (c-d) N-HCSs-50, respectively.

The relative concentration of the N configurations revealed that the N-HCSs-10 comprised of 24.8 % pyridinic-N, 41.5 % pyrrolic-N, 19.7 % graphitic-N and 14 % NO_x while the N-HCSs-50 had 34.7 % pyridinic-N, 48.2 % pyrrolic-N and 13.9 % graphitic-N and 3.2 % NO_x . This could suggest that in the N-HCSs surface, the nitrogen atoms are preferably attached at the defect vacancies generated via removal of amorphous carbon domains and sp^2/sp^3 carbon “dangling bonds” yielding the high pyrrolic-N and pyridinic-N contents. The representative structures of the different doped N-HCSs are shown in scheme 1.

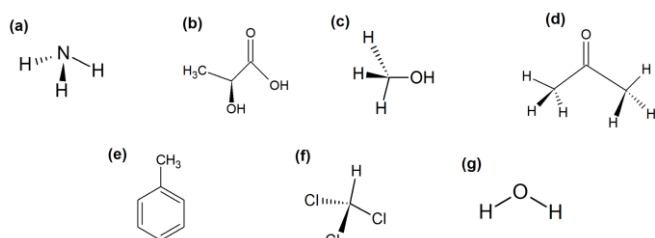


Scheme 1: Schematic representation of various N-configurations within (a) N-HCSs-10 and (b) N-HCSs-50.

3.3 Sensing properties of annealed HCSs and N-HCSs

Sensors were prepared from annealed HCSs, N-HCSs-10 and N-HCSs-50. The chemical sensing results presented in figure 4 show the results for ammonia, but similar results for all the

other analytes investigated are presented in figures S3-S8 (Supplementary Material). Figures 4 (a-c) show the sensor resistance as a function of the ammonia concentration. The sensor response ($\Delta R/R_0$) is presented in figures 4 (d-f) and further used to calculate the sensitivity (see Table 4). In all cases, the sensor response increased with increasing concentration. The resistance measurement frequency was selected based on two parameters: high magnitude of the response (figure 4(g-i)) and high SNR value (figure 4(j-l)).



Scheme 2: Structural formula for (a) ammonia, (b) lactic acid, (c) methanol, (d) acetone, (e) toluene, (f) chloroform, and (g) water molecules.

Our results show that our sensors prepared with annealed HCSs and N-HCSs respond to the presence of all investigated analytes; water, lactic acid, ammonia, methanol, acetone, toluene and chloroform. The concentration limit of detection (LoD) and sensitivities, S for the different analytes are shown in Table 4. Typically, the adsorption of a molecule on a carbon-based material is influenced by its polarity, vapour pressure, dipole moment as well as the porosity of the carbon surface^{72,73,74}. Polar analytes with high polarizability, high volatility (high vapour pressure) interact with functional groups on carbon surface more than their apolar counterparts. For instance, in the N-HCSs-based sensors, lower LoD limits were recorded for lactic acid, ammonia and water (polar groups).

These results suggested that the N-HCSs gave a lower limit of detection for water as compared to the annealed HCSs. This can be associated with the presence of nitrogen-induced defects in the N-HCSs surface that allowed for the interaction of the nitrogen-containing groups with the water molecules. However, the sensitivity (response as a function of analyte concentration) was lower meaning that the response and recovery towards the water molecules was slower compared to the annealed HCSs. We can postulate that there exists stronger interactions between the various oxygen and nitrogen-containing groups with the water molecules and this could reduce the response and recovery time yielding lower sensitivities. For the annealed HCSs, a higher limit of detection for water was displayed whilst the sensitivity was high. This could be due to the pure carbon surface (as confirmed by the TGA data), the presence of fewer oxygenated groups on the surface (as confirmed by the XPS data) and hence a weaker interaction of the carbon surface with water molecules.

Table 4: Frequency f , determined limit of detection concentration (LoD) and sensitivity, S for different analytes detection in sensors based on annealed HCSs and N-HCSs dispersion at 2 mg/mL concentration^a

Analyte		Annealed HCSs	N-HCSs-10	N-HCSs-50
Ammonia	f (kHz)	6	3	1
	LoD (ppm)	19	6	60
	S (ppm ⁻¹)	5.9×10^{-4}	5.2×10^{-4}	1.4×10^{-4}
Methanol	f (kHz)	6	1	6
	LoD (ppm)	40	54	64
	S (ppm ⁻¹)	2.4×10^{-4}	1.1×10^{-5}	1.8×10^{-4}
Toluene	f (kHz)	1	6	1
	LoD (ppm)	49	15	286
	S (ppm ⁻¹)	5.3×10^{-4}	8.7×10^{-4}	2.2×10^{-4}
Chloroform	f (kHz)	1	6	3
	LoD (ppm)	-	59.6	-
	S (ppm ⁻¹)	-	1.9×10^{-4}	-
Lactic acid	f (kHz)	6	20	6
	LoD (ppm)	28	15	12
	S (ppm ⁻¹)	2.3×10^{-2}	1.2×10^{-2}	4.1×10^{-2}
Water	f (kHz)	10	20	10
	LoD (ppm)	62	30	7
	S (ppm ⁻¹)	7.3×10^{-3}	2.4×10^{-3}	5.6×10^{-4}
Acetone	f (kHz)	3	6	10
	LoD (ppm)	-	-	83
	S (ppm ⁻¹)	-	-	2.0×10^{-3}

^aAbsent values could not be determined due to low signal to noise ratio

Moreover, the ammonia sensitivity (Table 1) of the HCSs-based sensors was better than that for methanol and chloroform vapours and this could be attributed to ammonia volatility (high vapour pressure) and the dipole-dipole interactions of the ammonia molecules with the carbon surface^{21,36}. In the case of the lactic acid, the C=O group could create an electron withdrawing effect on the electron-rich N-HCSs surface leading to a lower LoD value and better sensitivity⁷⁵. However, the methanol vapours showed lower LoD values for the annealed HCSs. It was noted that the N-HCSs-50 sensor gave lower sensitivities towards ammonia, methanol and toluene when compared to the annealed HCSs. This can be associated with an increase in the charge carrier density of the N-HCS sensor leading to a reduction of electrical resistance. Typically, ammonia molecules are considered to be electron donors while the presence of nitrogen-containing groups on the N-HCSs could create a cloud of electrons over the HCS surface. Consequently, an increase in the density of negative charge carriers, therefore, lowering the ammonia sensitivity. In the case of annealed HCSs, the absence of nitrogen-containing groups made them suitable electron acceptor sites for the ammonia molecules yielding higher ammonia sensitivity. Additionally, the carbon surface is also more conductive (I_D/I_G ratio: 0.51) and this allows easier interaction of the ammonia molecules with the carbon surface and hence higher sensitivity²¹.

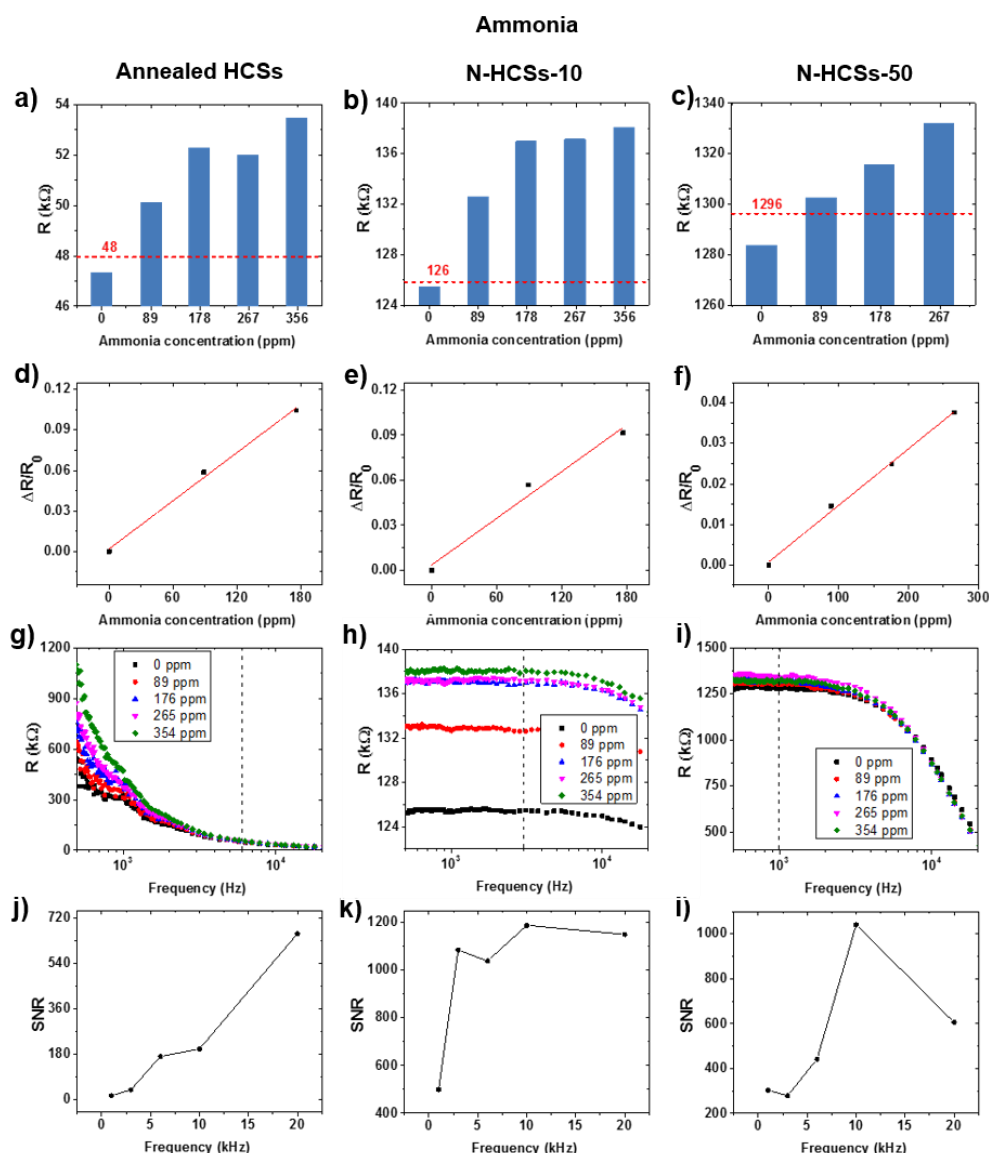


Figure 4: Sensor data for ammonia. (a-c) Sensor resistance as a function of analyte concentration, the red line indicates the estimated LoD resistance of the corresponding sensor; (d-f) response of the sensor versus analyte concentration; (g-i) sensor resistance dependence on frequency, dashed line indicates the working frequency; and (j-l) sensor signal to noise ratio (SNR) as a function of frequency. The results of sensors based on annealed HCSs, N-HCSs-10 and N-HCSs-50 are presented in the first, second and third column, respectively).

In the case methanol sensitivities, the N-HCSs showed lower sensitivities as compared to the annealed HCSs thus, following a similar trend reported by Greenshields *et al.*⁵² on N-MWCNT-PVA composites. Thus, further analysis of the methanol vapour detection behaviour of the N-HCSs based on the capacitive sensing mechanism will be of great interest. The N-HCSs-10 sensor gave the highest toluene sensitivity followed by annealed HCSs and N-HCSs-50, respectively. This was not unexpected as the N-HCSs-10 had lower LoD values than the N-HCSs-50. From literature, the N-MCNT-PVA composites were found to show high sensitivities towards low toluene concentration and vice-versa⁵².

In some cases saturation of the sensors was noted, when they were exposed to high concentrations of analytes (Figures S3-S8). In these cases, sensitivity was estimated using only the three lowest concentration values. It was not possible to identify a single frequency for which response and SNR were simultaneously high for all sensors and analytes. For this reason, the values presented in Table 4 are the values of sensor performance in the optimum operating frequency. Thus, neither a direct comparison between HCSs, N-HCSs-10 and HCSs-50 performance nor a correlation of performance and nitrogen content is possible using Table 4. For this reason, we present sensitivity values for all analytes determined at the same frequency of 6 kHz in Table 5, where some clear trends can be observed.

The increase in nitrogen content of the HCSs increased the sensitivity to lactic acid and decreased the sensitivity to water. This suggests enhanced interaction of the carbonyl and hydroxyl groups in lactic acid analyte with the oxidized nitrogen moieties (NO_x) and other nitrogen induced defects in the N-HCSs matrix as compared to the annealed HCSs surface. Due to the low signal to noise ratio, a trend could not be established for the sensing performance of the HCSs-based sensors towards apolar analytes.

Table 5: Sensitivity for different analytes of annealed HCSs, N-HCSs-10 and N-HCSs-50 based sensors at measurement frequency of 6 kHz

Analyte	Sensitivity (ppm ⁻¹)		
	Annealed HCSs	N-HCSs-10	N-HCSs-50
Ammonia	5.9×10^{-4}	1.4×10^{-4}	1.3×10^{-4}
Methanol	2.4×10^{-4}	7.9×10^{-5}	1.8×10^{-4}
Toluene	6.5×10^{-4}	8.7×10^{-4}	2.3×10^{-4}
Chloroform	-	1.9×10^{-4}	-
Lactic acid	2.3×10^{-2}	3.0×10^{-2}	4.1×10^{-2}
Water	0.3×10^{-1}	4.0×10^{-2}	3.0×10^{-3}
Acetone	-	-	1.5×10^{-4}

The annealed HCSs exhibited higher sensitivities towards ammonia, water and methanol vapours as compared to the N-HCSs. Indeed, water exhibited a clear sensitivity trend on N-content in HCSs, with the N-HCSs-50 showing the lowest sensitivity (Table 5). This indicated that ammonia post-synthesis N-doping and heat treatment of the HCSs aided in limiting the water vapour dependency of the N-HCSs sensors. This behaviour could be attributed to a moderate degree of graphitization for the N-HCSs (I_D/I_G ; 0.72) as compared to that of pristine HCSs²¹. Thus, annealing in ammonia served the dual role of removing any amorphous carbon domains as well as incorporating nitrogen defects on the HCSs surface. The reduction of sensitivity to water as the HCSs nitrogen content increases can be advantageous for application in sensor arrays for analyte discrimination in humid environments [21],

because it allows the separation of the water contribution to the sensors responses. However, the N-HCSs exhibited lower ammonia sensitivity than that reported previously for un-annealed HCSs²¹. This shows that the presence of a low content of O-N, O-C=O, C-N and C-O groups on the N-HCSs surface could impact on their vapour sensing properties^{76,77}. The sensitivity to ammonia also shows a clear tendency of reduction in the case of N-HCSs.

Our reported sensitivities of the annealed HCSs and N-HCSs towards toluene was higher than that reported in literature⁷⁸. For the water sensitives, our values were much lower than those of graphene oxide, graphene and pristine HCSs^{79,80,21} as highlighted in Table 6. This can be ascribed to the low oxygen content of the annealed HCSs and N-HCSs as compared to graphene oxide that typically contains a large number of oxygenated functional groups. The important point in this work is the low LoD values recorded for ammonia, methanol and toluene as compared to other reports in literature^{81,82,83,84}. Despite the low sensitivity towards ammonia, methanol and acetone vapours^{85,86,87,88,89}, the ability to limit water dependency of the N-HCSs sensors is of great significance to the future modification of carbon based chemical sensors.

The sensitivity values of the N-HCS based sensors can be compared to values reported by Rodrigues *et al.*⁹⁰. The N-HCSs based sensors showed significantly higher sensitivity than sensors based on β -In₂S₃ and rGO nanostructures for water and methanol molecules. Our previous study based on hollow carbon nanospheres and polyvinylpyrrolidone (HCSs/PVP) composites reported a sensitivity of up to two orders of magnitude higher at a controlled temperature (40 °C) and relative humidity²¹. This shows that with controlled temperature and relative humidity there is great potential to improve the chemical sensing properties of the N-HCSs. It is to be noted that even with the low nitrogen content reported in

Table 6: Comparative sensor data for the annealed HCSs and N-HCSs with other related materials in literature

Analyte	Material	Concentration (ppm)	Temperature	Sensitivity (ppm ⁻¹)	LoD (ppm)	Ref
Toluene	N-HCSs-10	0 - 463	RT	8.7×10^{-4}	15	This work
	MWCNTs	72 - 108	RT	2.8×10^{-5}	72	⁷⁸
	MWCNT/PEO			5.5×10^{-5}	72	
Water	Annealed HCSs	0 - 2025	RT	0.3×10^{-1}	62	This work
	N-HCSs-50			3.0×10^{-3}	7	
	Graphene	N/R	RT	3.0×10^{-1}	N/R	⁷⁹
	Graphene Oxide	N/R	RT	37800	N/R	⁸⁰
	Pristine HCSs	N/R	RT	199000	N/R	²¹
Ammonia	N-HCSs-10	0 - 354	RT	1.4×10^{-4}	6	This work
	RGO film	200-2800	RT	N/R	200	⁸¹
	Graphene foam	20- 1000	RT	N/R	20	⁸²
	RGO/TiO ₂ /Au	2-10	RT	1.43×10^{-2}	2	⁸⁵
Methanol	Annealed HCSs	0 - 1200	RT	2.4×10^{-4}	40	This work
	MWCNT/Au	15 - 40	RT	37.3×10^{-2}	NA	⁸⁶
	SnO ₂ /CNT	100-1000	200 °C	N/R	100	⁸³
	MIL-53(Cr-Fe)/Ag/CNT	10-500 ppm	RT	N/R	30.5 ppm	⁸⁴
Acetone	N-HCSs-50	0 - 480		1.5×10^{-4}	83	This work
	MWCNTs/Fe		RT	0.8×10^{-2}	N/R	⁸⁷
	HKUST-1 MOF (Cu ₃ (BTC) ₂ (H ₂ O)	N/R	RT	-	50 ppm	⁸⁹

this work (0.6 at. %), it was possible to control the humidity dependency of the HCSs and measure their sensitivity to both protic and aprotic analytes.

In this study, for the first time, the sensing properties of annealed HCSs and N-HCSs towards various chemical vapours is reported. The first indications that the type of N in the HCS plays a role in the sensing of analytes has been revealed. However, higher nitrogen contents in the HCSs will be necessary to understand the role of these various nitrogen configurations on the sensing properties of the HCSs. Our data also reveal that since our sensors showed a response to all tested analytes, a pattern recognition tool applied to a set of simultaneously operated sensors would be necessary for practical applications⁹¹.

4. Conclusions

Annealed HCSs and N-HCSs were successfully synthesized. The defect density induced on the HCSs increased with increasing dopant concentration. This was confirmed by the broad first order derivative peak (TGA data) and a higher I_D/I_G ratio (Raman data) seen in the N-HCSs-50 compared to the N-HCSs-10 and the annealed HCSs. The surface areas of all the HCSs were relatively low ($< 90 \text{ m}^2 \text{ g}^{-1}$) with a slight increase in the surface areas observed upon increasing the dopant concentration during the post-synthesis N-doping of the HCSs. The incorporation of nitrogen into the carbon matrix in the N-HCSs was confirmed by XPS spectra to be 0.2 at. % to 0.6 at. %, with a high percentage of pyridinic-N and pyrrolic-N. The annealed HCSs and N-doped carbons showed a potential application in chemical vapour sensors for the detection of ammonia, toluene, chloroform, lactic acid, water and acetone. Most importantly, the N-HCSs-50 exhibited lower sensitivity to water indicating the role of post-nitrogen doping and heat treatment of the HCSs in limiting the humidity dependency of the carbons. Thus, the N-HCSs-based sensors are candidates for humidity-independent devices for the sensing of volatile chemical vapours.

Conflicts of interest

There are no conflicts of interest to declare.

Acknowledgements

We thank the NRF, the University of Witwatersrand and the DST-NRF Centre of Excellence in Strong Materials for funding. We also thank the CNPq and the Federal University of Parana for financial support.

References

- 1 Z. Wen, Q. Wang, Q. Zhang and J. Li, *Electrochem. commun.*, 2007, **9**, 1867–1872.
- 2 X. Lai, J. E. Halpert and D. Wang, *Energy Environ. Sci.*, 2012, **5**, 5604–5618.
- 3 I. Nongwe, V. Ravat, R. Meijboom and N. J. Coville, *Appl. Catal. A Gen.*, 2013, **466**, 1–8.
- 4 C. H. Lee, K. M. Ho, F. W. Harris, S. Z. D. Cheng and P. Li, *Soft Matter*, 2009, **5**, 4914.
- 5 B. Jang, K. Yang, B. Quan and Y. Piao, *Mater. Lett.*, 2013, **104**, 68–71.
- 6 J. B. Joo, P. Kim, W. Kim, J. Kim, N. D. Kim and J. Yi, *Curr. Appl. Phys.*, 2008, **8**, 814–817.
- 7 P. Cai and L. Feng, *Mater. Chem. Phys.*, 2008, **108**, 1–3.
- 8 A.-H. Lu and F. Schüth, *Adv. Mater.*, 2006, **18**, 1793–1805.
- 9 H. Zhou, S. Li, Y. Wu, D. Chen, Y. Li, F. Zheng and H. Yu, *Sensors Actuators B Chem.*, 2016, **237**, 487–494.
- 10 H. Tamai, T. Sumi and H. Yasuda, *J. Colloid Interface Sci.*, 1996, **177**, 325–328.
- 11 J. Jang, X. L. Li and J. H. Oh, *Chem. Commun.*, 2004, **0**, 794.
- 12 G. Yang, R. Xu, M. Chen, X. Wang, L. Ling, R. Zhang and J. Yang, *New Carbon Mater.*, 2008, **23**, 205–208.
- 13 X. Chen, K. Kierzek, Z. Jiang, H. Chen, T. Tang, M. Wojtoniszak, R. J. Kalenczuk, P. K. Chu and E. Borowiak-Palen, *J. Phys. Chem. C*, 2011, **115**, 17717–17724.
- 14 B. Fang, J. H. Kim, M.-S. Kim, A. Bonakdarpour, A. Lam, D. P. Wilkinson and J.-S. Yu, *J. Mater. Chem.*, 2012, **22**, 19031.
- 15 Y. Dai, H. Jiang, Y. Hu, Y. Fu and C. Li, *Ind. Eng. Chem. Res.*, 2014, **53**, 3125–3130.
- 16 F. Su, X. S. Zhao, Y. Wang, L. Wang and J. Y. Lee, *J. Mater. Chem.*, 2006, **16**, 4413.
- 17 B. K. Mutuma, B. Matsoso, K. Ranganathan, D. Wamwangi and N. J. Coville, *RSC Adv.*, 2016, **6**, 20399–20408.
- 18 Zhiyong Wang, Fan Li, and Nicholas S. Ergang and A. Stein, 2006, *Chem. Mater.*, 2006, **18**, 5543–5553.
- 19 Q. Wang, J. Yan, Y. Wang, G. Ning, Z. Fan, T. Wei, J. Cheng, M. Zhang and X. Jing, *Carbon N. Y.*, 2013, **52**, 209–218.
- 20 N. A. Travlou and T. J. Bandoz, *Adsorption*, 2017, **23**, 271–280.
- 21 B. K. Mutuma, R. Rodrigues, K. Ranganathan, B. Matsoso, D. Wamwangi, I. A. Hümmelgen and N. J. Coville, *J. Mater. Chem. A.*, 2017, **5**, 2539–2549.
- 22 S. Gao, K. Geng, H. Liu, X. Wei, M. Zhang, P. Wang and J. Wang, *Energy Environ. Sci.*, 2015, **8**, 221–229.
- 23 V. Ravat, I. Nongwe and N. J. Coville, *ChemCatChem*, 2012, **4**, 1930–1934.
- 24 Zhuxian Yang, Yongde Xia, and Xuezhong Sun and R. Mokaya, *J. Phys. Chem. B.*, 2006, **110**, 18424–18431.
- 25 S. C. Ray, Z. N. Tetana, R. Erasmus, A. Mathur and N. J. Coville, *Int. J. Energy Res.*, 2014, **38**, 444–451.
- 26 H. Xiong, M. Moyo, M. A. Motchelaho, Z. N. Tetana, S. M. A. Dube, L. L. Jewell and N. J. Coville, *J. Catal.*, 2014, **311**, 80–87.
- 27 B. J. Matsoso, K. Ranganathan, B. K. Mutuma, T. Lerotholi, G. Jones and N. J. Coville, *RSC Adv.*, 2016, **6**, 106914–106920.
- 28 H.-C. Wen, K. Yang, K.-L. Ou, W.-F. Wu, C.-P. Chou, R.-C. Luo and Y.-M. Chang, *Surf. Coatings Technol.*, 2006, **200**, 3166–3169.
- 29 Yongde Xia, and Zhuxian Yang and R. Mokaya, *J. Phys. Chem. B.*, 2004, **108**, 19293–19298.
- 30 B. K. Mutuma, B. J. Matsoso, K. Ranganathan, J. M. Kheartland, D. Wamwangi and N. J. Coville, *RSC Adv.*, 2017, **7**, 21187–21195.
- 31 K. N. Wood, R. O’Hayre and S. Pylypenko, *Energy Environ. Sci.*, 2014, **7**, 1212–1249.
- 32 Paul H. Matter, Eugenia Wang, Maria Arias, and Elizabeth J. Biddinger and U. S. Ozkan, *J. Phys. Chem. B.*, 2006, **110**, 18374–18384.
- 33 P. Sun, K. Wang, J. Wei, M. Zhong, D. Wu and H. Zhu, *Nano Res.*, 2014, **7**, 1507–1518.
- 34 D. Guo, R. Shibuya, C. Akiba, S. Saji, T. Kondo and J. Nakamura, *Science*, 2016, **351**, 361–5.

- 35 B. J. Matsoso, B. K. Mutuma, C. Billing, K. Ranganathan, T. Lerotholi, G. Jones and N. J. Coville, *Electrochim. Acta.*, 2018, **286**, 29–38.
- 36 N. A. Travlou, M. Seredych, E. Rodríguez-Castellón and T. J. Bandoz, *Carbon N. Y.*, 2016, **96**, 1014–1021.
- 37 F. Villalpando-Páez, A. H. Romero, E. Muñoz-Sandoval, L. M. Martínez, H. Terrones and M. Terrones, *Chem. Phys. Lett.*, 2004, **386**, 137–143.
- 38 J.-J. Adjizian, R. Leghrib, A. A. Koos, I. Suarez-Martinez, A. Crossley, P. Wagner, N. Grobert, E. Llobet and C. P. Ewels, *Carbon N. Y.*, 2014, **66**, 662–673.
- 39 N. A. Travlou, C. Ushay, M. Seredych, E. Rodríguez-Castellón and T. J. Bandoz, *ACS Sensors.*, 2016, **1**, 591–599.
- 40 Y. Battie, O. Ducloux, P. Thobois, T. Susi, E. I. Kauppinen and A. Loiseau, *Phys. status solidi.*, 2011, **248**, 2462–2466.
- 41 L. He, B. Cui, J. Liu, Y. Song, M. Wang, D. Peng and Z. Zhang, *Sensors Actuators B Chem.*, 2018, **258**, 813–821.
- 42 L. Wang, T. Meng, J. Sun, S. Wu, M. Zhang, H. Wang and Y. Zhang, *Anal. Chim. Acta.*, 2019, **1047**, 28–35.
- 43 M. Liu, T. Zhang, H. Ren, L. Wang, T. Meng, J. Zhao, H. Wang and Y. Zhang, *Mater. Res. Bull.*, 2018, **104**, 15–19.
- 44 L. Fu, Y. Huang, H. Zhang, Y. Xie, W. Long, J. Yang, H. Shi and J. Ying, *Fullerenes, Nanotub. Carbon Nanostructures.*, 2018, **26**, 856–862.
- 45 L. Valentini, C. Cantalini, I. Armentano, J. M. Kenny, L. Lozzi and S. Santucci, *Diam. Relat. Mater.*, 2004, **13**, 1301–1305.
- 46 E. Gracia-Espino, B. Rebollo-Plata, H. Martínez-Gutiérrez, E. Muñoz-Sandoval, F. López-Urías, M. Endo, H. Terrones and M. Terrones, *J. Sensors.*, 2016, **2016**, 1–10.
- 47 W. Liu, L. Xu, K. Sheng, X. Zhou, B. Dong, G. Lu and H. Song, *NPG Asia Mater.*, 2018, **10**, 293–308.
- 48 T. W. Ebbesen and T. Takada, *Carbon N. Y.*, 1995, **33**, 973–978.
- 49 Y. Zhou, B. Wang, X. Song, E. Li, G. Li, S. Zhao and H. Yan, *Appl. Surf. Sci.*, 2006, **253**, 2690–2694.
- 50 P. C. P. Watts, N. Mureau, Z. Tang, Y. Miyajima, J. D. Carey and S. R. P. Silva, *Nanotechnology.*, 2007, **18**, 175701.
- 51 C. Cantalini, L. Valentini, I. Armentano, L. Lozzi, J. M. Kenny and S. Santucci, *Sensors Actuators B Chem.*, 2003, **95**, 195–202.
- 52 M. W. C. C. Greenshields, I. A. Hümmelgen, M. A. Mamo, A. Shaikjee, S. D. Mhlanga, W. A. L. van Otterlo and N. J. Coville, *J. Nanosci. Nanotechnol.*, 2011, **11**, 10211–10218.
- 53 J. A. Dean and N. A. Lange. *Lange's Handbook of Chemistry.*, New York: McGraw-Hill, 1999.
- 54 B. B. Cunha, M. W. C. C. Greenshields, M. A. Mamo, N. J. Coville and I. A. Hümmelgen, *J. Mater. Sci. Mater. Electron.*, 2015, **26**, 4198–4201.
- 55 L. Peng, J. Zhai, D. Wang, Y. Zhang, P. Wang, Q. Zhao and T. Xie, *Sensors Actuators B Chem.*, 2010, **148**, 66–73.
- 56 A. Shrivastava and V. Gupta, *Chronicles Young Sci.*, 2011, **2**, 21.
- 57 X. Li, H. Wang, J. T. Robinson, H. Sanchez, G. Diankov and H. Dai, *J. Am. Chem. Soc.*, 2009, **131**, 15939–15944.
- 58 T. Liu, T. Kou, D. Bulmahn, C. Ortuno-Quintana, G. Liu, J. Q. Lu and Y. Li, *ACS Appl. Energy Mater.*, 2018, **1**, 5043–5053.
- 59 W. Luo, B. Wang, C. G. Heron, M. J. Allen, J. Morre, C. S. Maier, W. F. Stickle and X. Ji, *Nano Lett.*, 2014, **14**, 26.
- 60 B. Stöhr, H. P. Boehm and R. Schlögl, *Carbon N. Y.*, 1991, **29**, 707–720.
- 61 C. Petit, K. Kante and T. J. Bandoz, *Carbon N. Y.*, 2010, **48**, 654–667.
- 62 J.-Y. Miao, D. W. Hwang, C.-C. Chang, S.-H. Lin, K. V. Narasimhulu and L.-P. Hwang, *Diam. Relat. Mater.*, 2003, **12**, 1368–1372.
- 63 A. C. Ferrari, *Solid State Commun.*, 2007, **143**, 47–57.
- 64 E. M. M. Ibrahim, V. O. Khavrus, A. Leonhardt, S. Hampel, S. Oswald, M. H. Rummeli and B. Büchner, *Diam. Relat. Mater.*, 2010, **19**, 1199–1206.
- 65 N. Dwivedi, S. Kumar, J. D. Carey, H. K. Malik and Govind, *J. Appl. Phys.*, 2012, **112**, 113706.
- 66 M. Thommes, *Chemie Ing. Tech.*, 2010, **82**, 1059–1073.
- 67 S. D. Mhlanga, N. J. Coville, S. E. Iyuke, A. S. Afolabi, A. S. Abdulkareem and N. Kunjuzwa, *J. Exp. Nanosci.*, 2010, **5**, 40–51.
- 68 L.-C. Chen, P.-Y. Peng, L.-F. Lin, T. C. K. Yang and C.-M. Huang, *Aerosol Air Qual. Res.*, 2014, **14**, 916–927.
- 69 J. Díaz, G. Paolicelli, S. Ferrer and F. Comin, *Phys. Rev. B.*, 1996, **54**, 8064–8069.
- 70 A. L. M. Reddy, A. Srivastava, S. R. Gowda, H. Gullapalli, M. Dubey and P. M. Ajayan, *ACS Nano*, 2010, **4**, 6337–6342.
- 71 H. Xiong, M. A. Motchelaho, M. Moyo, L. L. Jewell and N. J. Coville, *Appl. Catal. A Gen.*, 2014, **482**, 377–386.
- 72 M. M. Selim and T. A. El-Nabarawy, *Carbon N. Y.*, 1980, **18**, 287–290.
- 73 F. S. Dias, L. G. Tartuci, H. de F. Gorgulho and W. S. Machado, *Sensors Actuators B Chem.*, 2016, **231**, 440–449.
- 74 J. Choi, D. W. Park and S. E. Shim, *Macromol. Res.*, 2011, **980**, 980–983.
- 75 N. Lala, V. Thavasi, S. Ramakrishna, N. L. Lala, V. Thavasi and S. Ramakrishna, *Sensors.*, 2009, **9**, 86–101.
- 76 S. Giraudet, P. Pré, H. Tezel and P. Le Cloirec, *Carbon N. Y.*, 2006, **44**, 1873–1883.
- 77 N. A. Travlou, M. Seredych, E. Rodríguez-Castellón and T. J. Bandoz, *J. Mater. Chem. A.*, 2015, **3**, 3821–3831.
- 78 Y. Zhou, Y. Jiang, G. Xie, X. Du and H. Tai, *Sensors Actuators B Chem.*, 2014, **191**, 24–30.
- 79 A. D. Smith, K. Elgammal, F. Niklaus, A. Delin, A. C. Fischer, S. Vaziri, F. Forsberg, M. Råsander, H. Hugosson, L. Bergqvist, S. Schröder, S. Kataria, M. Östling and M. C. Lemme, *Nanoscale.*, 2015, **7**, 19099–109.
- 80 H. Bi, K. Yin, X. Xie, J. Ji, S. Wan, L. Sun, M. Terrones and M. S. Dresselhaus, *Sci. Rep.*, 2013, **3**, 2714.
- 81 R. Ghosh, A. Midya, S. Santra, S. K. Ray and P. K. Guha, *ACS Appl. Mater. Interfaces.*, 2013, **5**, 7599–7603.
- 82 F. Yavari, Z. Chen, A. V. Thomas, W. Ren, H.-M. Cheng and N. Koratkar, *Sci. Rep.*, 2011, **1**, 166.
- 83 C. Wongchoosuk, A. Wisitsoraat, A. Tuantranont and T. Kerdcharoen, *Sensors Actuators B Chem.*, 2010, **147**, 392–399.
- 84 M. Ghanbarian, S. Zeinali and A. Mostafavi, *Sensors Actuators B Chem.*, 2018, **267**, 381–391.
- 85 Y. Zhou, X. Li, Y. Wang, H. Tai and Y. Guo, *Anal. Chem.*, 2019, **91**, 3311–3318.
- 86 A. Thamri, H. Baccar, C. Struzzi, C. Bittencourt, A. Abdelghani and E. Llobet, *Sci. Rep.*, 2016, **6**, 35130.
- 87 P. Clément, I. Hafaiedh, E. J. Parra, A. Thamri, J. Guillot, A. Abdelghani and E. Llobet, *Carbon N. Y.*, 2014, **78**, 510–520.
- 88 Z. Liu, T. Yang, Y. Dong, X. Wang, Z. Liu, T. Yang, Y. Dong and X. Wang, *Sensors.*, 2018, **18**, 3113.
- 89 A. H. Khoshaman and B. Bahreyni, *Sensors Actuators B Chem.*, 2012, **162**, 114–119.
- 90 R. Rodrigues, *UNIVERSIDADE FEDERAL DO PARANÁ*, PhD Thesis, 2018, Brazil.
- 91 R. Rodrigues and I. A. Hümmelgen, *J. Solid State Electrochem.*, 2016, **20**, 1295–1301.